BOOSTING THE THERAPEUTIC EFFICACY OF DISCOIDAL NANOCONSTRUCTS AGAINST GLIOBLASTOMA WITH RATIONALLY DESIGNED PEG-DOCETAXEL CONJUGATES

Alessia Felici [1,2], Michele Schlich [1,3], Daniele Di Mascolo [1], Luca Goldoni [4], Anna Lisa Palange [1*], Paolo Decuzzi [1#*]

[1] Laboratory of Nanotechnology for Precision Medicine, Fondazione Istituto Italiano di Tecnologia, Genoa, 16163, Italy

[2] Department of Informatics, Bioengineering, Robotics and System Engineering, University of Genoa, Genoa, Italy

[3] Department of Life and Environmental Sciences, Università degli Studi di Cagliari. 09124 Cagliari, Italy

[4] Analytical Chemistry Laboratory, Fondazione Istituto Italiano di Tecnologia, 16163 Genova, Italy

[#] Corresponding author: paolo.decuzzi@iit.it
[*] These authors share the senior authorship

ABSTRACT

Maximizing loading while modulating the release of therapeutic molecules from nanoparticles and implantable drug delivery systems is key to successfully address deadly diseases like brain cancer. Here, four different conjugates of the potent chemotherapeutic molecule docetaxel (DTXL) were realized to optimize the pharmacological properties of 1,000×400 nm Discoidal Polymeric Nanoconstructs (DPNs). DTXL was covalently linked to poly-(ethylene) glycol (PEG) chains of different molecular weights, namely 350, 550 and 1,000 Da, and to oleic acid (OA). After extensive physico-chemical and pharmacological characterizations, the conjugate PEG_{550}-DTXL showed an optimal compromise between loading and sustained release out of the DPNs, as opposed to the insufficient loading of PEG_{1000}-DTXL and the excessively slow release of OA-DTXL. Not surprisingly, viability tests conducted on U87-MG cells showed a delay in cytotoxic activity for the DTXL conjugates compared to free DTXL within the first 48h. However, PEG_{550}–DTXL returned an IC_{50} value of ~9 nM at 72h, which is comparable to that of free DTXL. In mice bearing orthotopically implanted U87-MG cells, a treatment with PEG_{550}-DTXL loaded DPNs (1 mg/kg DTXL) was responsible for an overall animal survival of 52.5 days as opposed to 27 days resulting from the systemic administration of the clinical standard temozolomide (3 mg/kg). Collectively, these results continue to demonstrate that the therapeutic efficacy of nanoparticles can be boosted by rationally designing drug conjugates for optimal loading and release profiles.

INTRODUCTION

Currently, most chemotherapeutics used in the clinics are compounds with low molecular weight (MW) and a hydrophobic structure acting on the dysregulated cancer cell-mitotic machinery [1]. The small size and lipophilicity of these molecules certainly facilitate internalization into cells but also lead to poor bioavailability and fast renal clearance [2]. In addition, given the lack of specific targeting, treatments with these highly cytotoxic molecules are often restricted by dose-limiting systemic toxicity. At the same time, their low-dose and long-term use prompts the development of drug resistance by tumor cells. Among several chemotherapeutic molecules, docetaxel (DTXL) is considered one of the most potent. It arrests cell proliferation by promoting the formation of stable aggregates of microtubules [3, 4] and is commonly used for the treatment of advanced breast and ovarian cancer, and a wide range of other solid tumors. However, systemic toxicity of DTXL, including neutropenia, neuropathies, and hypersensitivity, limits its use as first line of treatment [5, 6]. In order to improve the safety profile, solubility and bioavailability, the DTXL molecule has been either modified with different biocompatible macromolecules to realize polymer-drug conjugates and micelles [5, 7] or directly incorporated into nanoparticles and various drug delivery systems. [8-15]

In the first case, several natural and synthetic polymers have been tested such as Hyaluronic acid (HA), albumin, carboxymethylcellulose, polysaccharide, PEG-PLA, PEG-PCC [16-21]. Among the different types of polymers already used, poly-(ethylene-glycol) (PEG) is the most popular option since its clinical value is well established [22, 23]. Indeed, as opposed to free drug molecules, PEG-drug conjugates could offer higher water solubility; increased bioavailability and circulation half-life; longer drug stability; and reduced antigenic activity. [24-26]. For PEG chains with a MW larger than DTXL (> 1,000 Da), the resulting amphiphilic conjugates tend to self-organize in core-shell structures upon dispersion in aqueous solution.

For instance, Liu et al. developed micelles by self-assembling of PEG_{2000} – DTXL molecules and demonstrated a 2-fold increase in blood longevity of DTXL as well as a 2.5-fold higher maximum tolerate dose as compared to the free drug.[27] More recently, a similar approach was followed by Guo and collaborators who demonstrated the conjugation of DTXL with poly (ethylene glycol)-poly (d,l-lactide-co-glycolide) block copolymer chains. The resulting 100 nm assemblies had higher cell internalization than free DTXL.[28] Despite the documented advantages of these PEG-DTXL conjugates over the free drug, one crucial limitation in generating conjugates with high MW PEG chains is the presence of multiple reactive positions and the poor conformational constrain that may result in loss of pharmaceutical activity [29, 30]. Differently, low MW PEG (< 1,000 Da) chains conjugated with DTXL through easter or amidic bonds do not affect the therapeutic efficacy of the resulting compound [31, 32]. Conversely, the PEG-DTXL conjugates resulting from low MW PEG do not self-assemble to form larger assemblies but, on the other hand, could be rationally designed to become payloads into nanoparticles and other drug delivery systems.

Over the last 20 years, a plethora of nanoparticles have been proposed for the encapsulation and delivery of multiple drug molecules, including docetaxel [8-13]. Most of these particles have a spherical shape, a characteristic size ranging between 100 and 200 nm, and, upon systemic administration, tend to lodge within a cancerous lesions exploiting the enhanced permeability and retention effect [33]. These nanoparticles are synthetized via a bottom-up approach relying on the self-assembling of individual molecular components and are composed of a variety of materials, including lipids, polymers, block copolymers and inorganic materials. A complementary delivery strategy has been more recently proposed by the authors and relies on discoidal polymeric nanoconstructs (DPNs), with a diameter of 1,000 nm and a height of 600 nm, made of entangled chains of poly (ethylene glycol)-diacrylate (PEG-DA) and poly lactic-

co-glycolic acid (PLGA). DPNs are realized via a top-down, template-based fabrication strategy that is responsible for the unique geometry and tunable deformability of the resulting particles.[34-36] These two features of DPNs – geometry and deformability – allow them to preferentially lodge within the malignant vasculature taking advantage of its high tortuosity, low blood perfusion and velocity [35, 37]. However, DPN deformability comes at the cost of a limited retention for small molecules within the PLGA/PEG matrix. Previous studies have shown that ~ 50% of the loaded DTXL molecules could be released within a few hours upon DPN incubation in a physiological solution.[38, 39]

In this work, various PEG-DTXL conjugates have been realized by reacting linear PEG chains, with a molecular weight ranging from 350 to 550, and 1,000 Da, with docetaxel molecules using a succinic acid spacer. After extensive physico-chemical and pharmacological characterizations, the best PEG-DTXL conjugate has been identified in terms of maximal loading and sustained release from DPNs. The therapeutic efficacy of DPNs carrying the optimal PEG-DTXL conjugates has been assessed in an orthotopic murine model of glioblastoma.

2. EXPERIMENTAL

2.1. Materials. Polydimethylsiloxane (PDMS) (Sylgard 184) was purchased from Dow Coming Corp (Midland, USA). Poly(vinylalcohol) (PVA, Mw 31,000 - 50,000), poly(DL-lactide-co-glycolide) acid (PLGA, lactide:glycolide 50:50, Mw 38,000-54,000), poly(ethylene glycol) diacrylate (Mn 750) (PEG DA), 2-hydroxy-4'-(2-hydroxyethoxy)-2-methylpropiophenone (photo-initiator), 4-(dimethylamino) pyridine (DMAP) (99%), succinic anhydride, triethylammine, dichloromethane anhydrous ≥99.8% (DCM) were purchased from Merck KGaA (Darmstadt, Germany). Docetaxel was purchased from Alfa Aesar

(Massachusetts, USA). Ammine-PEG 550, 350, and 1000 Da were purchased from creative PEGworks (Chapel Hill, USA). 1-Ethyl-3-(3-dimethylaminopropyl) carbodiimide (EDC) and N-hydroxysuccinimide (NHS) were purchased from Termo Fisher. All other solvents and reagents were purchased from Merck and used without further purification, unless specified.

METHODS

Fabrication of Discoidal polymeric nanoconstructs. Discoidal polymeric nanoconstructs (DPNs) were synthetized using a top-down fabrication strategy described in detail in previous works by the authors [36, 40]. Briefly, a silicon wafer that presents an array of cylindrical wells (diameter 1000 nm, height 400 nm) was used to prepare a negative replica of PDMS by casting. This PDMS replica was then used as a mold to obtain PVA templates presenting the same geometry of the original silicon master. DPNs were obtained by filling the 1000 x 400 nm wells in the PVA templates with a polymeric paste. This was composed of PLGA (50 mg) and PEG-DA (10 mg) dissolved in 1 mL DCM. The paste included also 0.6 mg of photo-initiator and the therapeutic payload of choice. 5 µL of such paste were spread over the PVA template using a razor blade to accurately fill each well. The so filled templates were exposed to UV light (366 nm) for crosslink the PEG-DA chains and, finally, dissolved in water to release the DPNs. These were further purified through multiple filtration and centrifugation steps as previously described.

Synthesis of 2' succinyl-docetaxel. Derivatization of docetaxel with ammine-terminated PEGs having different molecular weights required the prior formation of a docetaxel intermedia containing a carboxylic group, therefore 2' succinyl-docetaxel (s-DTXL) was synthetized as previously reported[41]. DTXL (50 mg, 6.19×10^{-5} mol) and DMAP (12.38×10^{-5} mol) were

dried under vacuum for two hours before starting the reaction to completely remove any trace of humidity. Then, the dried compounds were dissolved in 2 ml of anhydrous pyridine in a 25 ml round-bottom flask. The regents were stirred for a few minutes in nitrogen atmosphere at room temperature. Then, succinic anhydride dissolved in pyridine (1 eq) was added dropwise and left to react for 4 h under nitrogen atmosphere at room temperature to produce the product succinyl-docetaxel (s-DTXL). The reaction mixture was washed three times with Toluene and dried under low pressure to remove the pyridine and obtain a crystalline powder. The formation of s-DTXL conjugate was verified using ^{1}H nuclear magnetic resonance (NMR) and Liquid Chromatography with mass detention (UPLC-MS). The crude compound was dissolved in a minimal amount of dichloromethane and purified with automatic silica chromatography using a gradient of DCM (Solvent A) and DCM:Methanol (Solvent B, 9:1) to obtain only the mono-substituted derivate. The purification of the mono-substituted compound was monitored using UPLC-MS.

Synthesis of PEG-Docetaxel. Pure 2' succinyl-docetaxel (50 mg) was dissolved in anhydrous dichloromethane in a 50 ml round-bottom flask and was activated using EDC (1.2 eq) and NHS (1.2 eq) and triethylammine (TEA) for two hours under nitrogen atmosphere at room temperature. Then, amine-PEG (350, 550 or 1000 Da, 1 eq) was added into the reaction mixture and left overnight. The raw product was washed with DCM and dried at low pressure to remove residual tri-ethylamine (TEA). Then, it was dissolved in a minimal amount of dichloromethane and purified with automatic silica chromatography using a gradient of DCM (Solvent A) and DCM:Methanol (Solvent B, 9:1). The purity and structure consistency of the product was assessed by ^{1}H-NMR and Liquid Chromatography for mass detection (UPLC-MS).

CHEMICAL CHARACTERIZATION

NMR analysis. 5 mg of NMR sample was dissolved in 0.5 ml of $CDCl_3$ and transferred into 5 mm SampleJet disposable tubes (Bruker). NMR experiments were performed at 298 K on a Bruker AvanceIII 600 MHz spectrometer equipped with 5 mm QCI cryoprobe with z shielded pulsed-field gradient coil, and operating at 600.13 and 151.92 MHz, for ^{1}H and ^{13}C, respectively. ^{1}H NMR spectra were acquired, after having applied a 30 degree of flip angle, with 16 transients, 65,536 points of digitalization, 1s of inter-pulses delay over a spectral width of 20.03 ppm (offset positioned at 6.18 ppm). ^{13}C NMR experiments were performed with 25,600 scans, 32,768 digit points and 2 s of relaxation delay, over a spectral width of 240.1 ppm (offset at 100 ppm). Spectra were referred to not deuterated residual solvent peak, calibrated at 7.26 and 77.2 ppm for ^{1}H and ^{13}C respectively. In bold are reported the diagnostic ^{1}H and ^{13}C signals, which unambiguously identify the derivatives (or the position of substitution), see also **Figure 2**.

Docetaxel ^{1}H NMR δ 8.10 (d, *J* 7.59 Hz, 2H), 7.61 (m, 1H), 7.50 (m, 2H), 7.40 (m, 2H), 7.38 (m, 2H), 7.32 (m, 1H), 6.21 (*br t*, *J* 8.30 Hz, 1H), 5.68 (d, *J* 7.09 Hz, 1H), 5.43 (d, *J* 9.03 Hz, 1H), 5.26 (d, *J* 8.04 Hz, 1H), 5.20 (s, 1H), 4.94 (m, 1H), **4.62(*br* s, 1H),** 4.31 and 4.19 (AB, d, *J* 8.55 Hz, 2H), 4.23 (m, 1H), 3.91 (d, *J* 7.03 Hz, 1H), 3.37(br s,1H), 2.58 and 1.84 (AB, m, 2H), 2.37(s, 3H), 2.27 (m, 2H), 1.85 (s, 3H), 1.76 (s, 3H), 1.34 (s, 9H), 1.24 (s, 3H), 1.13 (s, 3H) ppm. ^{13}C NMR δ 211.6, 172.9, 170.5, 167.2, 155.5, 138.6, 138.5, 136.1, 133.9, 130.3, 129.3, 129.0, 128.9, 128.2, 126.9, 84.3, 81.2, 80.4, 79.0, 76.8, 74.9, 74.7, 73.8, 72.6, 72.2, 57.8, 56.3, 46.6, 43.2, 37.2, 35.9, 28.3, 26.6, 22.7, 20.8, 14.5, 10.0 ppm.

2′ Succinyl-docetaxel ^{1}H NMR δ 8.10 (brs, 2H), 7.62 (m, 1H), 7.50 (m, 2H), 7.38 (m, 2H), 7.30 (d, *J* 7.72 Hz, 2H), 7.29 (m, 1H), 6.20 (br s, 1H), 5.66 (m, 1H), 5.56 (m, 1H), 5.45 (m, 1H), **5.38 (d, *J* 3.6 Hz 1H),** 5.23 (m, 1H), 4.95 (m, 1H), 4.30 and 4.18 (AB, m, 2H), 4.24 (m,

1H), 3.88 (br s, 1H)**, 2.79 (m, 2H), 2.63 (m, 2H)**, 2.55 and 1.86 (AB, m, 2H), 2.41(br s, 3H), 2.28 and 2.14 (AB, m, 2H), 1.92 (br s, 3H), 1.77(s, 3H), 1.34 (br s, 9H), 1.20 (s, 3H), 1.11 (s, 3H) ppm. ^{13}C NMR δ 211.5, **175.1**, **171.6**, 170.1, 168.3, 167.2, 155.4, 139.3, 137.4, 135.7, 133.9, 130.3, 129.4, 129.0, 128.8, 128.4, 126.6, 84.4, 81.2, 80.6, 79.6, 76.7, 75.1, 74.8, 74.6, 72.2, 71.9, 57.8, 54.3, 46.6, 43.2, 36.9, 35.6, **28.9**, **28.7**, 28.3, 26.5, 22.7, 20.9, 14.3, 10.1 ppm.

PEG350-docetaxel ^{1}H NMR δ 8.10 (d, *J* 7.51 Hz, 2H), 7.60 (m, 1H), 7.50 (m, 2H), 7.37 (m, 2H), 7.30 (m, 2H), 7.28 (m, 1H), **6.66 (br s, 1H, NH)**, 6.18 (br s, 1H), 5.67 (m, 1H), 5.59 (m, 1H), 5.42 (m, 1H), 5.27 (m, 1H), 5.23 (m, 1H), 4.95 (d, *J* 9.14 Hz 1H), 4.30 and 4.18 (AB, m, 2H), 4.25 (m, 1H), 3.89 (br s, 1H), **3.63 (m, 24H), 3.54 (m, 4 H), 3.42 (m, 2H), 3.37 (br s, 3H)**, 2.73 (m, 2H), 2.56 and 1.86 (AB, m, 2H)**, *2.46 (brs, 2H),*** 2.41(br s, 3H), 2.29 and 2.14 (AB, m, 2H), 1.93 (br s, 3H), 1.73 (br s, 3H), 1.34 (br s, 9H), 1.20 (s, 3H), 1.11 (s, 3H) ppm. ^{13}C NMR δ 211.6, 172.1, **171.9**, 171.2, 168.3, 167.2, 155.4, 139.2, 137.6, 135.7, 134.0, 130.3, 129.4, 129.0, 128.8, 128.3, 126.7, 84.4, 81.1, 80.4, 79.0, 76.7, 75.1, 74.7, 74.6,72.0, **7**1.7, **70.5**, 70.3, 69.9, **59.2**, 57.7, 54.4, 46.6, 43.2, **39.5**, 37.0, 35.6, 30.6, 29.8, 29.3, 28.3, 26.5, 22.8, 21.0, 14.4, 10.1 ppm.

PEG550-docetaxel ^{1}H NMR δ 8.10 (d, *J* 7.51 Hz, 2H), 7.60 (m, 1H), 7.50 (m, 2H), 7.37 (m, 2H), 7.30 (m, 2H), 7.29 (m, 1H), **6.65 (br s, 1H, NH)**, 6.19 (br s, 1H), 5.67 (m, 1H), 5.59 (m, 1H), 5.41 (m, 1H), 5.27 (m, 1H), 5.23 (m, 1H), 4.95 (d, *J* 9.16 Hz 1H), 4.30 and 4.17 (AB, m, 2H), 4.25 (m, 1H), 3.89 (br s, 1H**), 3.63 (m, 19H), 3.54 (m, 4 H), 3.42 (m, 2H), 3.37 (br s, 3H)**, 2.73 (m, 2H), 2.55 and 1.86 (AB, m, 2H), **2.47 (brs, 2H**), 2.39(br s, 3H), 2.28 and 2.14 (AB, m, 2H), 1.93 (br s, 3H), 1.73 (br s, 3H), 1.33 (br s, 9H), 1.20 (s, 3H), 1.11 (s, 3H) ppm. ^{13}C NMR δ 211.6, 172.1, **172.0**, 171.2, 168.3, 167.2, 155.4, 139.2, 137.6, 135.7, 134.0, 130.3, 129.4, 129.0, 128.8, 128.3, 126.7, 84.4, 81.1, 80.4, 79.0, 76.7, 75.1, 74.7, 74.6, 72.0, **7**1.7, **70.5**, 70.3, 69.9, **59.2**, 57.7, 54.4, 46.6, 43.2, **39.5**, 37.0, 35.6, 30.6, 29.8, 29.3, 28.3, 26.5, 22.8, 21.0, 14.4, 10.1 ppm.

PEG1000-docetaxel ^{1}H NMR δ 8.10 (d, *J* 7.23 Hz, 2H), 7.61 (m, 1H), 7.50 (m, 2H), 7.38 (m, 2H), 7.30 (m, 2H), 7.29 (m, 1H), **6.65 (br s, 1H, NH)**, 6.19 (br s, 1H), 5.67 (m, 1H), 5.59 (m, 1H), 5.43 (m, 1H), 5.27 (m, 1H), 5.23 (m, 1H), 4.95 (d, *J* 9.01 Hz 1H), 4.30 and 4.17 (AB, m, 2H), 4.25 (m, 1H), 3.89 (br s, 1H**), 3.63 (m, 22H), 3.54 (m, 4 H), 3.42 (m, 2H), 3.37 (br s, 3H)**, 2.74 (m, 2H), 2.55 and 1.86 (AB, m, 2H), **2.47 (brs, 2H**), 2.40 (br s, 3H), 2.29 (m, 2H), 1.92 (br s, 3H), 1.74 (br s, 3H), 1.33 (br s, 9H), 1.21 (s, 3H), 1.11 (s, 3H) ppm. ^{13}C NMR δ 211.6, 172.0, **171.8**, 171.1, 168.3, 167.2, 155.4, 139.2, 137.6, 135.7, 133.8, 130.3, 129.4, 129.0, 128.8, 128.3, 126.6, 84.4, 81.1, 80.4, 79.0, 76.7, 75.1, 74.7, 74.6, 72.0, **7**1.8, **70.7**, 70.3, 69.9, **59.2**, 57.7, 54.4, 46.6, 43.2, **39.5**, 37.0, 35.6, 30.7, 29.8, 29.3, 28.3, 26.5, 22.8, 21.0, 14.4, 10.1 ppm.

Mass spectroscopy. UPLC –MS analyses were run on a Waters ACQUITY UPLC-MS system consisting of a SQD (single quadrupole detection) mass spectrometer equipped with an electron spray ionization interface and a photodiode array detector. The PDA range was 210-400 nm.

DPNs morphological characterization. The quality and yielding of DPN synthesis were assessed through Multisizer 4E Coulter Particle Counter (Beckman Coulter, USA), using 20 µl of particles suspension in 20 mL of isotone solution. The hydrodynamic diameter and surface electrostatic charge (ζ – potential) of DPN was measured using a Zetasizer Nano (Malvern, UK). The characteristic discoidal shape of DPN was confirmed using Electron Microscopy. The DPN morphology before and after drug loading was observed using a Jem-1011 Transmission Electron Microscope (Jeol, Japan) and Scanning Electron Microscopy (Helios Nanolab 650) after 10 nm aurum coating.

Loading and Release studies. The direct loading method was used to incorporate PEG_{350}-DTXL, PEG_{550}-DTXL, or PEG_{1000}-DTXL within the DPN matrix. DTXL-loaded DPNs were also prepared as a reference. Different amounts of PEG-DTXL (or DTXL) were dissolved in the polymeric paste (0.5, 1, 2 and 10 mg/ml) to screen the best conditions for the loading process. To determine the encapsulation efficiency, DPNs were separated from the free drug by centrifugation at 12,700 rpm for 20 minutes and removing the supernatant. The pelleted particles were dried under vacuum overnight and dissolved in acetonitrile. The obtained solution was injected in a HPLC system (Agilent 1260 Infinity, Germany) coupled with UV detector for the quantification of DTXL or its conjugates (detected at 230 nm). The column used was a Zorbax RRHd Eclipse Plus C18 2.1x100 mm, 1.8 µm and the mobile phase consisted of a mixture of acetonitrile and water (53:47 v/v), with flow set at 0.3 ml/min. Release studies were performed under infinite sink physiological conditions with a 4L buffer receptor phase at controlled pH of 7.4 and temperature of 37° C. A 200 µL of DPN solution was poured into Slide-A-Lyzer MINI dialysis cups with a molecular cut off of 10 kDa (Thermo Scientific) and dialyzed over time up to 72h. At fixed time of 0, 1h, 3h, 8h, 24 h, 48h, 72h, the samples (n=3 replicates per time point) were withdraw from cups and centrifuged to collect DPNs. The pellet was dried, dissolved in acetonitrile and analyzed by HPLC as described above for the loading studies.

In vitro cell viability tests. The human glioblastoma cell line U87-MG was obtained from the American Type Culture Collection (ATCC). Cells were cultured in Eagle's minimal essential medium (EMEM) (ATCC, USA) completed with 10% FBS (Gibco, Thermo Fisher Scientific, USA), 1% penicillin/streptomycin (Sigma-Aldrich, USA), under a humid atmosphere (37°C, 5% CO_2, 95% air). *In vitro* cell viability was determined by MTT assay, which detected the reduction of MTT (3-(4,5-dimethylthiazolyl)-2,5-diphenyltetrazolium bromide) (Sigma-Aldrich, USA) by mitochondrial dehydrogenase to blue formazan product. This reflected the normal function of mitochondria and, hence, cell viability. Different number of cells were seeded in 96-well plates for each time point, specifically 10^4 cells/well for the 24h, $7.5x10^3$ for 48h, and $5\ x10^3$ for 72h and 96h. The day after, cells were treated with PEG_{350}-DTXL, PEG_{550}-DTXL or PEG_{1000}-DTXL dissolved in DMSO and diluted with complete medium to yield concentrations between 1 and 1,000 nM. Treatments with DTXL or s-DTXL using the same conditions were also performed as controls. After 24, 48, 72, or 96h the treatments were removed, and cells incubated for 3 hours with complete medium containing MTT (0.25 mg/ml). The resulting formazan crystals were then dissolved in ethanol (200 μL/well) and the absorbance was read at 570 nm using a microplate reader (Tecan, CH). The effect of PEG_{550}-DTXL-loaded DPNs on cell viability was also evaluated employing the same procedure, dispersing the DPN, loaded with a known amount of compound, in the cell culture medium to achieve the desired drug concentration in the wells (1-1000 nM). Six replicates were considered for each drug concentration. Data were collected when the absorbance ranged between 0.2 and 1.2. Cell viability was normalized with respect to untreated cells.

Tumor model and therapeutic experiments. All animal experiments were performed according to the guidelines established by the European Communities Council Directive (Directive 2010/63/EU of 22 September 2010) and approved by the National Council on

Animal Care of the Italian Ministry of Health. All efforts were made to minimize animal suffering and use the lowest possible number of animals required to produce statistical relevant results, according to the "3Rs concept". For the orthotopic intracranial GBM tumor model, 5-6 week-old female athymic nude mice were used (Charles River, Calco, Italy). Animals were grouped in ventilated cages and able to freely access food and water. They were maintained under controlled conditions: temperature (21 ± 2 °C), humidity (50 ± 10%) and light (12 and 12 h of light and dark, respectively). Before cells injection, animals were anaesthetized with a mixture of ketamine (10%) and xylazine (5%), which was administered via a single intraperitoneal injection. For the injection, trypsinized $5x10^5$ U87-MG luciferase positive cells were resuspended in cold phosphate-buffered saline. A total of 3 ul of PBS was injected into the right hemisphere of the mouse brain (1.5 mm posterior to the bregma, 1.4 mm lateral to the midline, and 1 mm depth from skull) at a speed of 0.3 μL/min using a 10 μL sterile Hamilton syringe fitted with a 26-gauge needle attached to a stereotaxic frame. Wounds were closed with sterile wound clips and animals were carefully monitored until recovered from anesthesia. Tumor growth was followed by IVIS every 2 days, upon intraperitoneal injection of D-luciferin, Potassium salt (GoldBio) at a dose of 150 mg/kg. On day 15, before starting the treatments, a bigger hole of about 3 mm was created in the same stereotactic coordinates by using a Trephine - 2.7mm Diameter. The more superficial part of the tumor was resected by using a scalpel. The skull was then sealed by a drop of silicon elastomer. IVIS was performed the day after the surgery to assess tumor resection. Mice were then randomly divided into three experimental groups: saline, free TMZ and PEG_{550}DTXL-DPNs, intravenously injected at a dose of 1 mg/kg every other day. The effectiveness of the different treatments was evaluated by optical imaging (IVIS) every two days. All mice were euthanized when they became moribund. Survival was monitored and plotted using the Kaplan-Meier method. Log-rank test was used to test the significance of different survival curves.

2.10 Statistical analysis. All data were processed using Excel 2010 software (Microsoft) and GraphPad PRISM. Results are expressed as mean + standard deviation. Statistical analyses on *in-vivo* experiments were performed using t-test. Log-rank test was used to test the significance of different survival curves. The p-values of <0.05 (*), <0.01 (**), and <0.001 (***) were considered to be statistically significant.

3 RESULTS AND DISCUSSION

3.1 Fabrication and biopharmaceutical characterization of docetaxel-loaded DPN. Discoidal Polymeric Nanoconstructs (DPN) are particles made of polylactic-co-glycolic acid (PLGA) and polyethylene glycol diacrylate (PEG-DA) chains entangled together to form a circular polymeric disc of 1,000 × 400 nm. These nanoconstructs are obtained via a top-down, template-based fabrication strategy as depicted in **Figure 1A,B** and previously described by the authors[40]. Specifically, 1,000 × 400 nm discoidal wells, realized in a sacrificial PVA template, are carefully filled with a polymeric paste containing 40 kDa PLGA chains and 700 Da PEG-DA chains dissolved in chloroform in the mass ratio 5:1. After solvent evaporation and PVA dissolution in a water bath, DPN are collected via centrifugation. The two polymers composing the DPN entangle each other forming a network of hydrophobic and hydrophilic pockets, where small molecules can be readily entrapped[42]. Indeed, hydrophobic drugs, like the chemotherapeutic agent docetaxel (DTXL), can be mixed within the PLGA/PEG polymeric paste and directly encapsulated in the resulting DPN. However, differently from conventional PLGA nano and microparticles obtained by nanoprecipitation or emulsion techniques, DPN present a relatively high-porosity matrix from which even the ~800 Da DTXL can be released quite rapidly. **Figure 1C** shows the percentage of encapsulated DTXL released out of DPN over time under physiological conditions (PBS, pH 7.4, temperature of 37° C). Note that over 40% of the loaded DTXL is released within the first 2h, and this number grows to almost 80%

already at 10h. This is an indirect demonstration of the higher porosity of the DPN, as compared to conventional PLGA microspheres whose release rates are typically lower [43].

In order to modulate the release profile of small molecules out of DPN, the authors previously conjugated lipid chains, like oleic acid (OA), to DTXL. This resulted in a highly hydrophobic complex with a significant reduction in release rate as compared to molecular DTXL (**Figure 1C**). However, the OA-DTXL complex was so impermeable to water molecules to prevent any hydrolysis and final release of free DTXL, with inevitable consequences on therapeutic efficacy. Based on this data, here the authors decided to focus on the realization of PEG-DTXL conjugates using PEG chains with a molecular weight comparable to that of DTXL, namely 350, 550 and 1,000 Da. This is indeed different from what already documented in the literature where DTXL is directly conjugated with high molecular weight PEG chains (> 2 kDa) [44]

3.2 Synthesis and Characterization of PEG-DTXL conjugates. The conjugation of PEG-DA chains with DTXL was realized using a succinic acid spacer in a panel of two-step reactions (**Figure 2A**). In the first step, succinic anhydride was directly conjugated to the hydroxyl group of DTXL (s-DTXL), with highest preference for the hydroxyl group in C2' (2'C-OH). Indeed, the comparison of the ^{1}H NMR docetaxel spectrum with the one recorded after the reaction with succinic anhydride, show the eclipse of 2'CH-OH signal, at 4.63 ppm, and the appearance of a new peak, at 5.39 ppm (**Figure 2B**). The ^{1}H signal (but not the correspondent ^{13}C) is low fielded shifted, which is characteristic of hydroxyl esterification in agreement with those reported in literature [45]. Furthermore, the risk of multiple substitutions was limited using 1 eq of succinic acid and purification of the intermedia with automatic silica chromatography. The purity of the product was assessed by UPLC-MS spectra reporting M+1:908. In the second step, the pure s-DTXL was reacted separately with PEG_{350}, PEG_{550}, PEG_{1000}. ^{1}H NMR spectra confirmed the reaction completion reporting both the peaks at 3.63 ppm, characteristic of the

ethylene repetition, and at 6.65 ppm, a signature of the new amidic bond (inserts in **Figure 2B**). ^{1}H and ^{13}C NMR signals of all derivatives are described in M and M section with diagnostic signals in bold. Furthermore, UPLC-MS spectrum showed a characteristic bell-shaped distribution as a results of the ethylene repetition (+44) around the calculated molecular weights.

3.3 PEG-DTXL conjugates in DPN. The three different PEG-DTXL conjugates were directly loaded into DPN during the fabrication process. After loading and proper washings, the geometrical and physico-chemical proprieties of the drug-loaded DPN were assessed using a Zetasizer Nano, a Multisizer particle counter and electron microscopy (**Figure 3A – C**). Regardless of the molecular size of the loaded PEG-DTXL conjugate, the geometry of DPN was preserved returning a characteristic size diameter of about 1,000 nm. No statistically significant different in size distribution profile was detected via the Zetasizer nano and Multisizer characterizations. No statistically significant difference in surface electrostatic potential ζ was also detected. Numerical data for these physical quantities are listed in the table of **Figure 3**. The discoidal shape of DPN was confirmed via electron microscopy imaging (**Figure 3C**), which, interestingly, documented the presence of spherical aggregates at the water/particle interface. The size of these aggregates appeared to grow with the PEG molecular weight and is in line with previous reports describing, at least for PEG chains larger than 2,000 Da, the self-assembling of DTXL-PEG conjugates into larger structures [44]. Indeed, these structures can be more visible on the surface of the particles than within their polymeric core. Altogether, these data confirmed that the encapsulation of PEG-DTXL conjugates in the DPN does not alter their overall morphology.

3.4 Bio-Pharmaceutical properties of PEG-DTXL conjugates in DPN. The loading of DTXL in DPN is expressed in terms of µg of DTXL per billions of DPN, as shown in **Figure 4A**, for all tested configurations. For DTXL, loading was very poor with over 90% of the input amounts being likely lost during the last DPN fabrication and purification steps, including the dissolution of the sacrificial PVA template in water and particle collection via centrifugation. Indeed, both steps expose DPN to large amounts of water for a few hours, during which small molecules can readily migrate away from the DPN matrix. Then, the hydrophobic conjugate (OA-DTXL) were considered. The amount of drug loaded significatively increases reaching 56 ± 10 µg. Then, PEG-DTXL conjugates were considered. Interestingly, at low PEG-DTXL input amounts (<< 10 mg/ml), the loading continued to be poor with more than 90% loss. However, at higher input amounts (10 mg/ml), PEG_{550}-DTXL showed a loading efficiency much higher than for free DTXL. Specifically, 41 ± 15 µg of PEG_{550}-DTXL were loaded per billion of DPN with a 4-fold improvement as compared to free DTXL. The loading was lower for the PEG_{350}-DTXL, being just 2 times higher than DTXL (21 ± 17 µg per billion of DPN). Interestingly, no significant difference in loading was documented between PEG_{1000}-DTXL (~6 ± 3 µg per billion of DPN) and free DTXL.

Following the loading characterizations, release studies were performed by incubating DPN in 4 liters of PBS to reproduce the infinite sink conditions. The burst release observed for the molecular DTXL within the first hour post incubation (**Figure 1C**) was significantly reduced for the PEG-DTXL conjugates. This is more clearly shown in **Figure 4B** and its inset, where, at 2h, ~40% of free DTXL was already released as opposed to ~30% for PEG_{350}-DTXL, ~20% for PEG_{550}-DTXL, and ~10% for PEG_{1000}-DTXL. Similarly, at 24h, almost 80% of the free DTXL was released against 60% for the shorter PEG conjugates. The PEG_{1000}-DTXL was more tightly retained within the polymeric matrix of DPN with only 20% of the loaded dose

being released. At 72h, the amounts of released DTXL were 80%, 70% and 40% for the PEG_{350}-DTXL, PEG_{550}-DTXL and PEG_{1000}-DTXL.

Indeed, the addition of PEG chains increases the steric hindrance of the conjugates, as opposed to the free DTXL molecule, in a PEG molecular weight dependent manner. On one side, excessively short PEG chains do not provide a significant increase in steric hindrance (350 Da PEG vs 800 Da DTXL), thus explaining the relatively low loading and fast release rate. It is indeed likely that most PEG_{350}-DTXL could be washed out of the DPN already during the last purification steps, just like is the case of the free DTXL. On the other side, excessively long PEG chains (1,000 Da PEG vs 800 Da DTXL) tend to form large micellar structures that are less efficiently encapsulated into DPN (low loading) and, those few conjugates that are loaded inside the DPN matrix are more slowly released. It is indeed likely that most $PEG_{1,000}$-DTXL could not even be loaded into DPN but would rather loosely adsorb on the DPN surface and be washed away during the last purification steps. PEG_{550} appears to provide the optimum combination to maximize loading while returning a sustained DTXL release. In the sequel, only PEG_{550}-DTXL loaded DPN are considered, given the superior performance of this conjugate.

3.5 Cell cytotoxicity of PEG-DTXL conjugates and DPN. The cytotoxic activity of free DTXL, PEG-DTXL conjugates and DPN was assessed against a glioblastoma cell line (U87-MG) (**Figure 5 A-D**). In general, the treatment with PEG-DTXL conjugates provided a delayed response as compared to free DTXL. Specifically, the IC_{50} at 24h ranged between 20 and 40 times higher for the PEG-DTXL conjugates than for DTXL, as listed in the table of **Figure 5F**. However, these early-time-point differences in IC_{50} were observed to diminish and become negligible at longer time points. This delay is related to the progressive hydrolysis of the PEG complex that is required to expose the hydroxyl group in position 2'C of the DTXL molecule (**Figure 2A**). This group is important for the pharmacological activity of DTXL but it is also

used to link the succinic-PEG chains [46]. Interestingly, also the s-DTXL showed a delayed activity which, differently from the PEG-DTXL conjugates, stays lower for a longer time. This might be related to the presence of an anionic charge on the free carboxyl group of the s-DTXL, which limits its ability to diffuse across biological membrane and enter cells. As the PEG_{550}-DTXL showed the best encapsulation efficiency and a suitable release rate from DPN, next the cytotoxic activity of PEG_{550}-DTXL loaded DPN was evaluated. As expected, the encapsulation of PEG conjugates within DPN led to a delay in activity (**Figure 5E, F**), resulting from the combination of the PEG-DTXL release and its hydrolyzation [47]. However, the full advantage of DTXL-DPNs over free DTXL can be explicitly appreciated only upon conducting *in vivo* therapeutic experiments.

3.6 Therapeutic efficacy of PEG_{550}-DTXL loaded DPN. The glioma cell line U87-MG Luc+ was injected into the prefrontal cortex 0.75 mm from the skull and left to grow until an average radiance of ~10^6, which is associated with a stable tumor growth based on previous data by the authors [8]. Treatments were initiated after resecting the main tumor. Three experimental groups were considered, namely the gold standard temozolomide (iv TMZ – 3 mg/kg); PEG_{550}-DTXL loaded DPN (only 1 mg/kg of DTXL); and saline solution (CTRL). All the treatments were administered intravenously every other day over a period of 20 days, as schematically shown in **Figure 6A**. The treatment with PEG_{550}-DTXL loaded DPN slowed down significantly the progression of the disease as compared to TMZ and CTRL (**Figure 6B**). More informative are the Kaplan–Meyer curves of **Figure 6C** showing that all the untreated mice (CTRL) succumbed within 30 days post study initiation; TMZ treated mice lived longer, even though, as expected, returned a median survival of 27 days, equal to the saline group. Finally, the treatment with DPN was able to extend the mice overall survival up to 52.5 days. The success of the DPN therapy over the control experiments should be ascribed to the ability of the particles

to reach the malignant vasculature and release PEG_{550}-DTXL conjugates that, after passing the blood brain barrier, induce death in the rapidly replicating cancer cells. To assess the intratumor accumulation of DPN, an *in vivo* optical imaging analyses was also performed on DPN labeled with the near-infrared compound DSPE-Cy5. Results presented in **Figure 6D** show a side-by-side comparison between the bioluminescence signal of the U87-MG Luc+ tumor cells (left panel) and the fluorescence signal associated with the Cy5-DPN (right panel) confirming the accumulation of the polymeric nanoconstructs within tumor vasculature. Indeed, additional studies will be carried out to assess quantitatively the accumulation of DPN and DTXL within the malignant brain vasculature and tumor parenchyma, respectively.

CONCLUSIONS

In conclusion, this work demonstrates that Discoidal Polymeric Nanoconstructs can be engineered to deliver hydrophilic compounds, such as OA-DTXL and free DTXL, as well as PEG-conjugates of DTXL. Specifically, the potent chemotherapeutic agent – docetaxel – has been conjugated with PEG chains of different molecular weights, ranging from 350 to 1,000 Da. A systematic analysis on the loading and release of free DTXL and its various conjugates out of DPN has allowed the authors to identify PEG_{550}-DTXL as the most effective compound with an optimal compromise between sustained release and encapsulation efficiency. Although, PEG-DTXL conjugates presented a delayed cytotoxic activity in vitro as compared to free DTXL, due to the slower release and need to hydrolyze the PEG-DTXL bond, the PEG_{550}-DTXL DPN successfully extended the survival of mice bearing an orthotopically implanted glioblastoma model from 27 to 52.5 days. This data continues to demonstrate the efficacy of the DPN platform in treating tumors more efficiently than free chemotherapeutic molecules.

ACKNOWLEDGMENTS

This project was partially supported by the European Research Council, under the European Union's Seventh Framework Programme (FP7/2007-2013)/ERC grant agreement no. 616695 and by the European Union's Horizon 2020 research and innovation programme under the Marie Skłodowska-Curie grant agreement No 754490. The authors acknowledge the precious support provided by the Analytical Chemistry, Material Characterization, Nanofabrication and Animal facilities at the Italian Institute of Technology.

REFERENCES

1. Gaillard, H., T. García-Muse, and A. Aguilera, *Replication stress and cancer*. Nature Reviews Cancer, 2015. **15**(5): p. 276-289.
2. Lipinski, C.A., *Drug-like properties and the causes of poor solubility and poor permeability.* Journal of pharmacological and toxicological methods, 2000. **44**(1): p. 235-249.
3. Jordan, M., *Mechanism of action of antitumor drugs that interact with microtubules and tubulin.* Current Medicinal Chemistry-Anti-Cancer Agents, 2002. **2**(1): p. 1-17.
4. Checchi, P.M., et al., *Microtubule-interacting drugs for cancer treatment.* Trends in pharmacological sciences, 2003. **24**(7): p. 361-365.
5. ten Tije, A.J., et al., *Pharmacological effects of formulation vehicles: implications for cancer chemotherapy.* Clin Pharmacokinet, 2003. **42**(7): p. 665-685.
6. Weiss, R.B., et al., *Hypersensitivity reactions from taxol.* Journal of clinical oncology, 1990. **8**(7): p. 1263-1268.
7. Zhao, P. and D. Astruc, *Docetaxel nanotechnology in anticancer therapy.* ChemMedChem, 2012. **7**(6): p. 952.

8. Di Mascolo, D., et al., *Tuning core hydrophobicity of spherical polymeric nanoconstructs for docetaxel delivery.* Polymer International, 2016. **65**(7): p. 741-746.

9. Farokhzad, O.C., et al., *Targeted nanoparticle-aptamer bioconjugates for cancer chemotherapy in vivo.* Proc Natl Acad Sci U S A, 2006. **103**(16): p. 6315-20.

10. Hrkach, J., et al., *Preclinical development and clinical translation of a PSMA-targeted docetaxel nanoparticle with a differentiated pharmacological profile.* Sci Transl Med, 2012. **4**(128): p. 128ra39.

11. Gaucher, G., R.H. Marchessault, and J.C. Leroux, *Polyester-based micelles and nanoparticles for the parenteral delivery of taxanes.* J Control Release, 2010. **143**(1): p. 2-12.

12. Liu, Y., et al., *Folic acid conjugated nanoparticles of mixed lipid monolayer shell and biodegradable polymer core for targeted delivery of Docetaxel.* Biomaterials, 2010. **31**(2): p. 330-8.

13. Xu, Z., et al., *The performance of docetaxel-loaded solid lipid nanoparticles targeted to hepatocellular carcinoma.* Biomaterials, 2009. **30**(2): p. 226-32.

14. Di Mascolo, D., et al., *Conformable hierarchically engineered polymeric micromeshes enabling combinatorial therapies in brain tumours.* Nat Nanotechnol, 2021.

15. Gok, B., et al., *Adjuvant treatment with locally delivered OncoGel delays the onset of paresis after surgical resection of experimental spinal column metastasis.* Neurosurgery, 2009. **65**(1): p. 193-9; discussion 199-200.

16. Wang, W., et al., *Dendronized hyaluronic acid-docetaxel conjugate as a stimuli-responsive nano-agent for breast cancer therapy.* Carbohydrate Polymers, 2021. **267**: p. 118160.

17. Ernsting, M.J., et al., *Synthetic modification of carboxymethylcellulose and use thereof to prepare a nanoparticle forming conjugate of docetaxel for enhanced cytotoxicity against cancer cells.* Bioconjugate chemistry, 2011. **22**(12): p. 2474-2486.

18. Almawash, S.A., G. Mondal, and R.I. Mahato, *Coadministration of polymeric conjugates of docetaxel and cyclopamine synergistically inhibits orthotopic pancreatic cancer growth and metastasis.* Pharmaceutical research, 2018. **35**(1): p. 1-13.

19. Shi, L., et al., *Docetaxel-conjugated monomethoxy-poly (ethylene glycol)-b-poly (lactide)(mPEG-PLA) polymeric micelles to enhance the therapeutic efficacy in oral squamous cell carcinoma*. RSC advances, 2016. **6**(49): p. 42819-42826.

20. Evans, C.W., et al., *Synthetic copolymer conjugates of docetaxel and in vitro assessment of anticancer efficacy.* New Journal of Chemistry, 2020. **44**(46): p. 20013-20020.

21. Etrych, T.s., et al., *HPMA copolymer conjugates of paclitaxel and docetaxel with pH-controlled drug release.* Molecular pharmaceutics, 2010. **7**(4): p. 1015-1026.

22. Ekladious, I., Y.L. Colson, and M.W. Grinstaff, *Polymer–drug conjugate therapeutics: advances, insights and prospects.* Nature Reviews Drug Discovery, 2019. **18**(4): p. 273-294.

23. Duncan, R., *The dawning era of polymer therapeutics.* Nature reviews Drug discovery, 2003. **2**(5): p. 347-360.

24. Abuchowski, A., et al., *Effect of covalent attachment of polyethylene glycol on immunogenicity and circulating life of bovine liver catalase.* Journal of Biological Chemistry, 1977. **252**(11): p. 3582-3586.

25. Li, C. and S. Wallace, *Polymer-drug conjugates: recent development in clinical oncology.* Advanced drug delivery reviews, 2008. **60**(8): p. 886-898.

26. Pasut, G. and F. Veronese, *Polymer–drug conjugation, recent achievements and general strategies.* Progress in polymer science, 2007. **32**(8-9): p. 933-961.

27. Liu, J., et al., *Nano-sized assemblies of a PEG-docetaxel conjugate as a formulation strategy for docetaxel.* J Pharm Sci, 2008. **97**(8): p. 3274-90.

28. Guo, Y., et al., *Reduction-Sensitive Polymeric Micelles Based on Docetaxel-Polymer Conjugates Via Disulfide Linker for Efficient Cancer Therapy.* Macromol Biosci, 2016. **16**(3): p. 420-31.

29. Lim, S.M., et al., *Enhancement of docetaxel solubility using binary and ternary solid dispersion systems.* Drug development and industrial pharmacy, 2015. **41**(11): p. 1847-1855.

30. Hamidi, M., P. Rafiei, and A. Azadi, *Designing PEGylated therapeutic molecules: advantages in ADMET properties.* Expert opinion on drug discovery, 2008. **3**(11): p. 1293-1307.

31. Hoste, K., K. De Winne, and E. Schacht, *Polymeric prodrugs.* International journal of pharmaceutics, 2004. **277**(1-2): p. 119-131.

32. Banerjee, S.S., et al., *Poly (ethylene glycol)-prodrug conjugates: concept, design, and applications.* Journal of drug delivery, 2012. **2012**.

33. Maeda, H., *Toward a full understanding of the EPR effect in primary and metastatic tumors as well as issues related to its heterogeneity.* Advanced drug delivery reviews, 2015. **91**: p. 3-6.

34. Key, J., et al., *Soft Discoidal Polymeric Nanoconstructs Resist Macrophage Uptake and Enhance Vascular Targeting in Tumors.* ACS Nano, 2015. **9**(12): p. 11628-41.

35. Palange, A.L., et al., *Deformable Discoidal Polymeric Nanoconstructs for the Precise Delivery of Therapeutic and Imaging Agents.* Mol Ther, 2017. **25**(7): p. 1514-1521.

36. Palomba, R., et al., *Modulating phagocytic cell sequestration by tailoring nanoconstruct softness.* ACS nano, 2018. **12**(2): p. 1433-1444.

37. Felici, A., et al., *Vascular-confined multi-passage discoidal nanoconstructs for the low-dose docetaxel inhibition of triple-negative breast cancer growth.* Nano Research, 2021: p. 1-10.

38. Felici, A., et al., *Vascular-confined multi-passage discoidal nanoconstructs for the low-dose docetaxel inhibition of triple-negative breast cancer growth.* Nano Research, 2022. **15**(1): p. 482-491.

39. Ferreira, M., et al., *Optimizing the Pharmacological Properties of Discoidal Polymeric Nanoconstructs Against Triple-Negative Breast Cancer Cells.* Front Bioeng Biotechnol, 2020. **8**: p. 5.

40. Ferreira, M., et al., *Optimizing the pharmacological properties of discoidal polymeric nanoconstructs against triple-negative breast cancer cells.* Frontiers in bioengineering and biotechnology, 2020. **8**: p. 5.

41. Dosio, F., et al., *Preparation, characterization and properties in vitro and in vivo of a paclitaxel–albumin conjugate.* Journal of Controlled Release, 1997. **47**(3): p. 293-304.

42. Pannuzzo, M., et al., *Predicting the Miscibility and Rigidity of Poly (lactic-co-glycolic acid)/Polyethylene Glycol Blends via Molecular Dynamics Simulations.* Macromolecules, 2020. **53**(10): p. 3643-3654.

43. Rafiei, P. and A. Haddadi, *Docetaxel-loaded PLGA and PLGA-PEG nanoparticles for intravenous application: pharmacokinetics and biodistribution profile.* International journal of nanomedicine, 2017. **12**: p. 935.

44. Liu, J., et al., *Nano-sized assemblies of a PEG-docetaxel conjugate as a formulation strategy for docetaxel.* Journal of pharmaceutical sciences, 2008. **97**(8): p. 3274-3290.

45. Huynh, L., J.-C. Leroux, and C. Allen, *Enhancement of docetaxel solubility via conjugation of formulation-compatible moieties.* Organic & biomolecular chemistry, 2009. **7**(17): p. 3437-3446.

46. Fu, Y., et al., *Medicinal chemistry of paclitaxel and its analogues.* Current medicinal chemistry, 2009. **16**(30): p. 3966-3985.

47. Fang, Y., et al., *Cleavable PEGylation: a strategy for overcoming the "PEG dilemma" in efficient drug delivery.* Drug Delivery, 2017. **24**(2): p. 22-32.

Figure

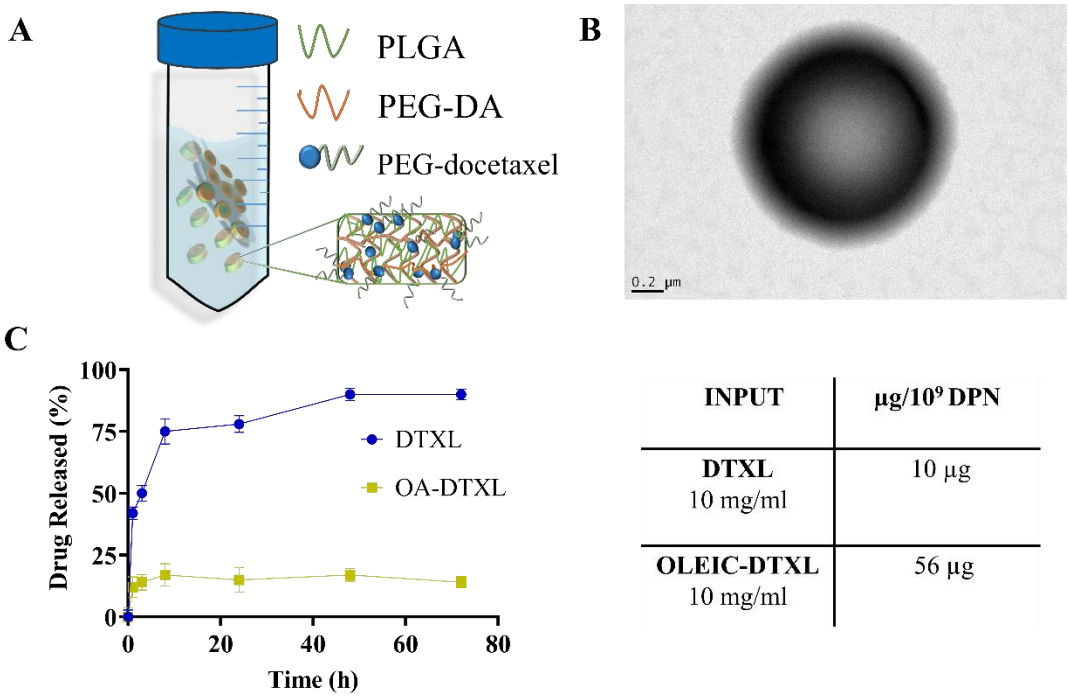

INPUT	µg/10^9 DPN
DTXL 10 mg/ml	10 µg
OLEIC-DTXL 10 mg/ml	56 µg

Figure 1. Discoidal polymeric Nanoconstructs (DPN). A. Schematic representation of the final steps in DPN manufacturing – release from the polyvinyl alcohol (PVA) sacrificial template and collection via centrifugation. **B.** Transmission Electron microscopy image of a DPN. **C**. Release profiles for free DTXL and OA-DTXL directly encapsulated into DPN and amounts of encapsulated drug molecules per billions of DPN (table on the right).

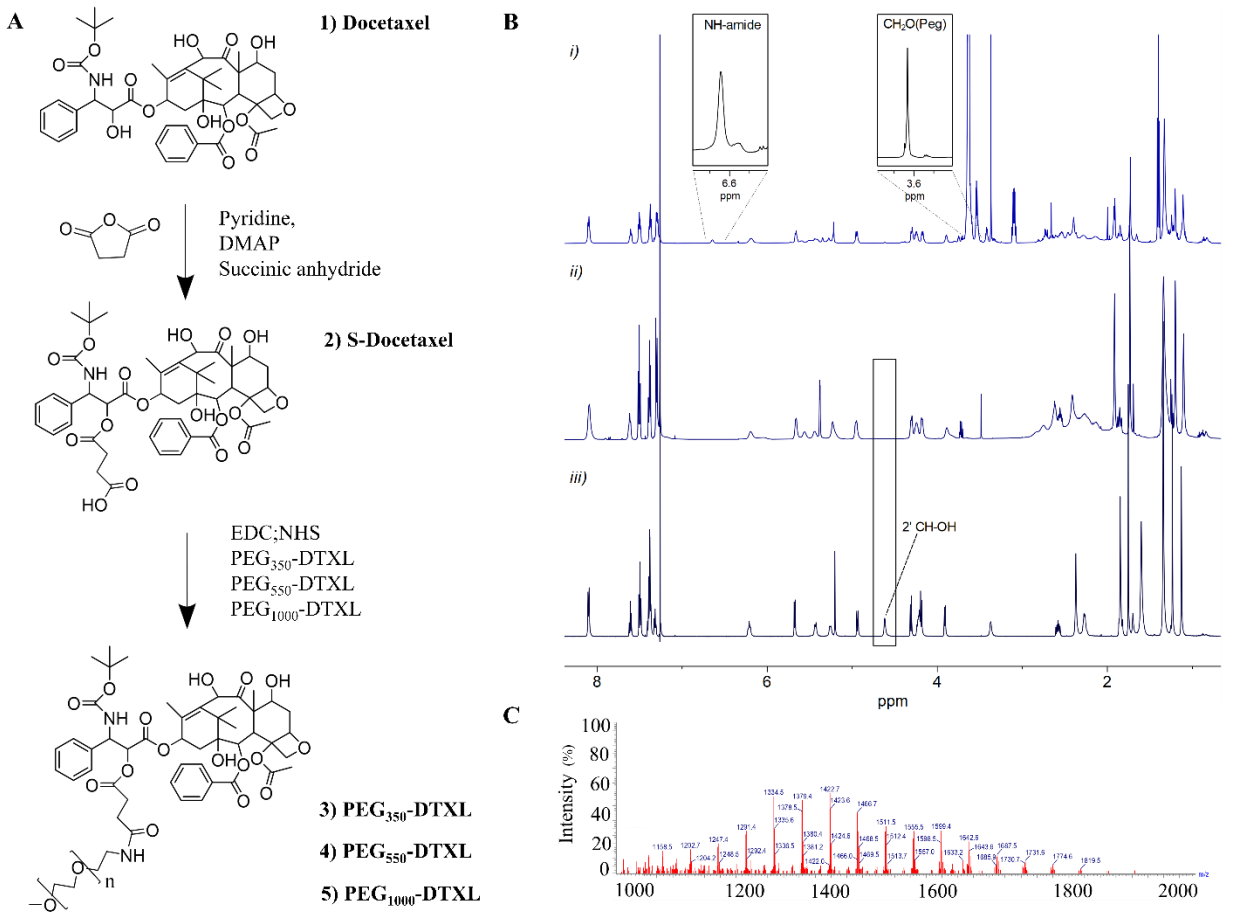

Figure 2. Synthesis and characterization of PEG-DTXL conjugates. A. Synthetic routes for the preparation of PEG-DTXL complexes; **B**. ^{1}H-NMR spectra in $CDCl_3$ of PEG_{1000}-DTXL(i) with the insets reporting the amide signal at 6.65 ppm and the CH_2O of PEG moieties demonstrating unambiguously the reaction with both the succinic and PEG moieties, S-DTXL(ii), DTXL (iii). The disappearance of the signal at 4.62 ppm in the spectrum ii (i.e. 2'CH-OH of docetaxel iii) demonstrates the regio-chemistry of esterification. **C.** UPLC-MS representative spectrum reported for PEG_{550}-DTXL

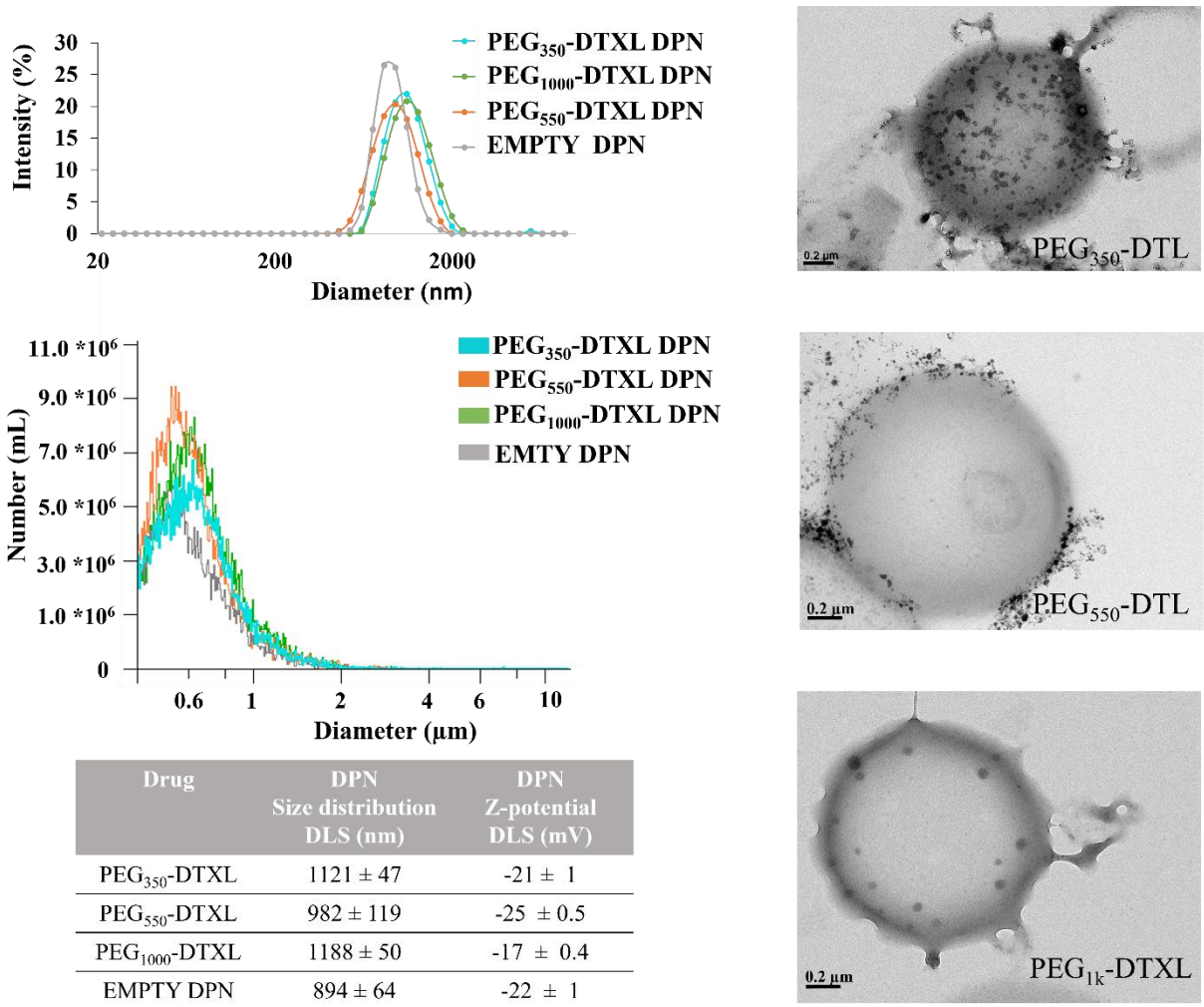

Drug	DPN Size distribution DLS (nm)	DPN Z-potential DLS (mV)
PEG_{350}-DTXL	1121 ± 47	-21 ± 1
PEG_{550}-DTXL	982 ± 119	-25 ± 0.5
PEG_{1000}-DTXL	1188 ± 50	-17 ± 0.4
EMPTY DPN	894 ± 64	-22 ± 1

Figure 3. Morphological characterization of DTXL-loaded DPN. A. Size distribution of empty DPNs and DPNs loaded with PEG350-DTXL, PEG550-DTXL and PEG1000-DTXL via dynamic light scattering **B.** Size distribution of empty DPNs and DPNs loaded with PEG350-DTXL, PEG550-DTXL and PEG1000-DTXL via Multisizer Coulter Counter. **C.** Table summarizing size and surface ζ-potential for all formulations (n=3) **D.** Morphological characterization of the particles after loading using Transmission Electron Microscopy.

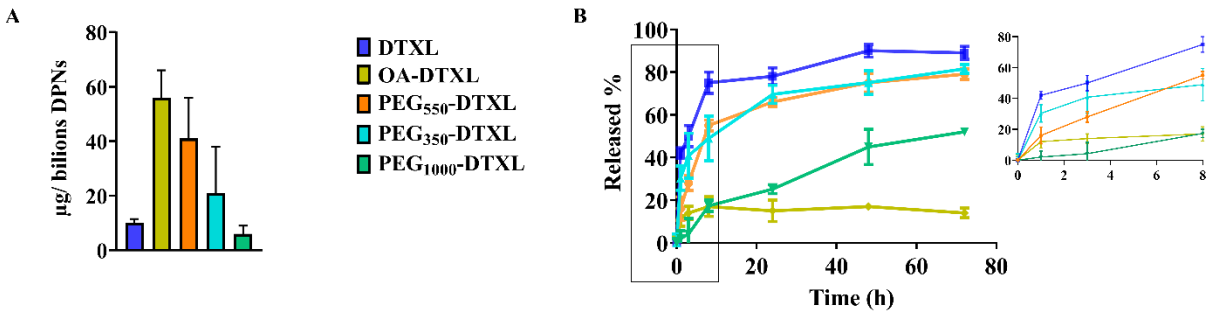

Input	DTXL	OA-DTXL	PEG_{550}-DTXL	PEG_{350}-DTXL	PEG_{1000}-DTXL
10 mg/ml	10 µg ± 1.5	56 µg ± 10	41 µg ± 15	21 µg ± 17	6 µg ± 3

Figure 4. BioPharmaceutical properties of PEG-DTXL conjugates in DPN. A. Encapsulation efficiency of DTXL, OA-DTXL and PEG-DTXL conjugates in DPN, expressed as total mass of DTXL per billions of DPN, for different drug inputs (n=3) **B**. Release profile of DTXL and PEG-DTXL conjugates from DPNs under the infinite sink conditions (at pH = 7.4 and 37° C) (n=3) **C.** Total loaded mass per DPN configuration for a given input of DTXL (n = 3).

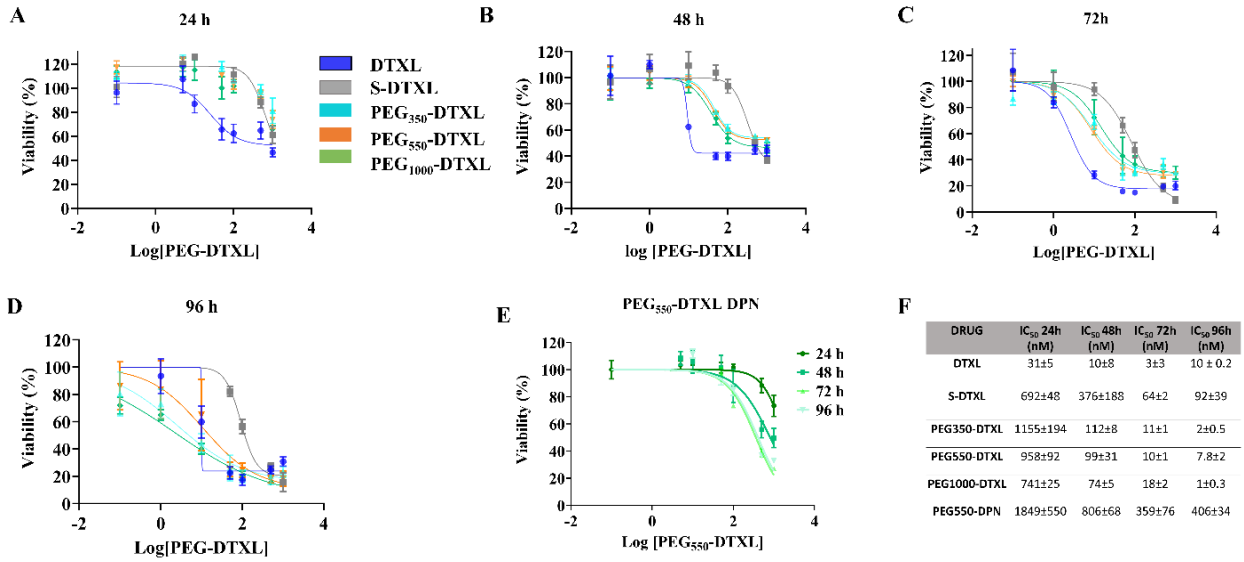

DRUG	IC_{50} 24h (nM)	IC_{50} 48h (nM)	IC_{50} 72h (nM)	IC_{50} 96h (nM)
DTXL	31±5	10±8	3±3	10 ± 0.2
S-DTXL	692±48	376±188	64±2	92±39
PEG350-DTXL	1155±194	112±8	11±1	2±0.5
PEG550-DTXL	958±92	99±31	10±1	7.8±2
PEG1000-DTXL	741±25	74±5	18±2	1±0.3
PEG550-DPN	1849±550	806±68	359±76	406±34

Figure 5. Cell cytotoxicity of PEG-DTXL conjugates and DPNs. A, B, C, D. Cell viability, expressed as percentage of residual metabolic activity, upon incubation with DTXL, S-DTXL or PEG-DTXL conjugates for 24, 48, 72 or 96 hours, respectively (n=6). **E.** Cell viability upon incubation with PEG_{550}-DTXL DPN (n=6). **F.** Table summarizing the IC_{50} values of the various treatment groups.

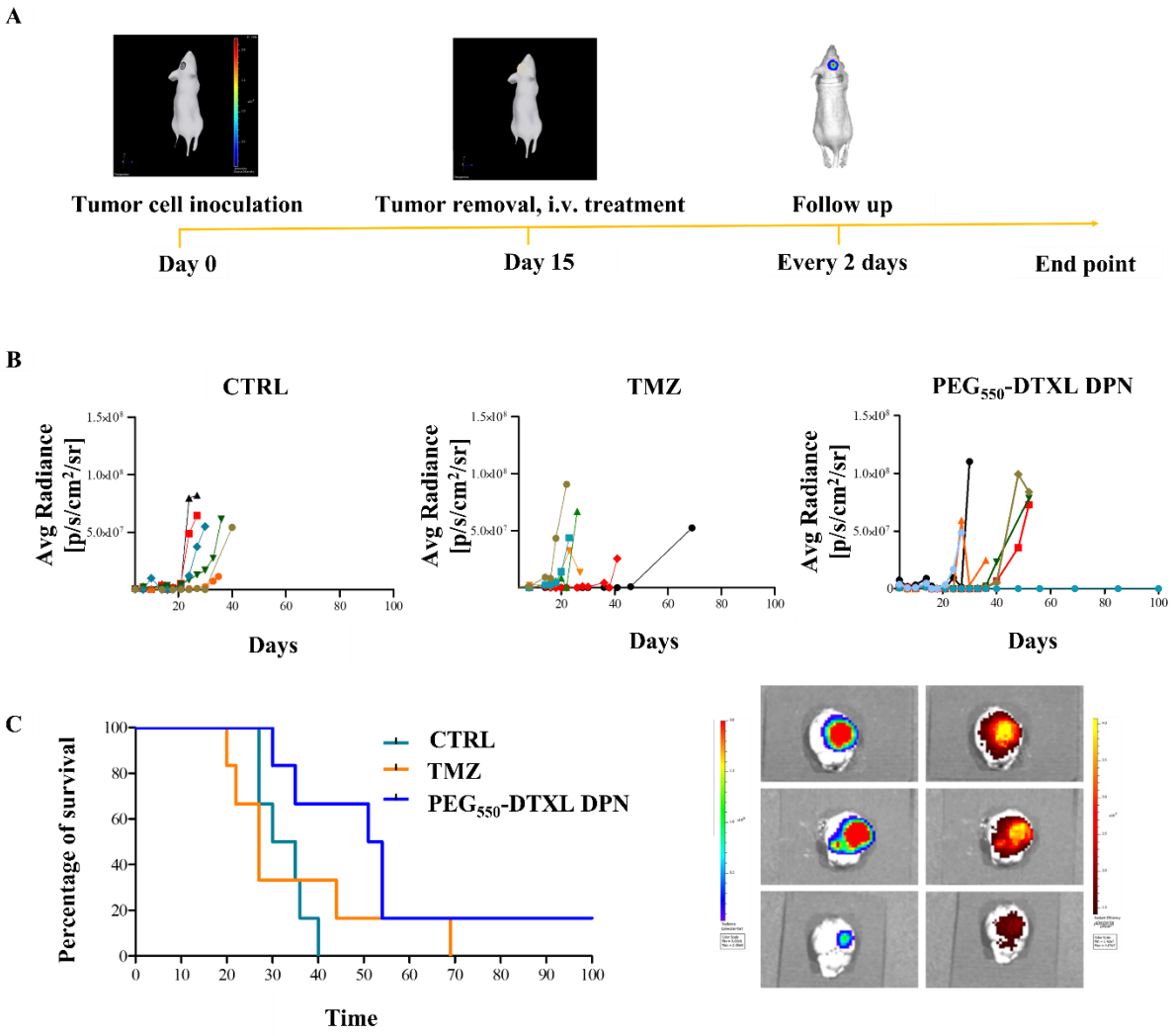

Figure 6. Therapeutic efficacy of PEG_{550}-DTXL loaded DPN on glioblastoma murine models. A. Timeline of the preclinical experiments performed on mice bearing orthotopically implanted brain cancer cells. **B.** Average radiance of the single mice for each experimental group. **C.** Kaplan–Meier curves for survival (green line: saline; orange line: free TMZ; blue line: PEG-DTXL-DPN). **D.** ex vivo bioluminescence and fluorescence analysis for brain tumors harvested at 24 h post Cy5-DPN injection.